Nano Energy 119 (2024) 109054

Contents lists available at ScienceDirect

Nano Energy

journal homepage: www.elsevier.com/locate/nanoen

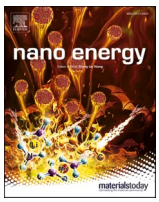

Full paper

Ultra-thin and high-voltage-stable Bi-phasic solid polymer electrolytes for high-energy-density Li metal batteries

Yiqi Gong [a], Changhong Wang [b], Mingyang Xin [a], Silin Chen [a], Pingbo Xu [a], Dan Li [a], Jia Liu [a], Yintong Wang [c], Haiming Xie [a,*], Xueliang Sun [d,*], Yulong Liu [a,*]

[a] National & Local United Engineering Laboratory for Power Battery, Department of Chemistry, Northeast Normal University, Changchun 130024, China
[b] Eastern Institute for Advanced Study, Eastern Institute of Technology, Ningbo, Zhejiang 315200, China
[c] Department of Theoretical and Applied Mechanics, Tsinghua University, Beijing100084, China
[d] Department of Mechanical and Materials Engineering, University of Western Ontario, London, Ontario N6A 5B9, Canada

ARTICLE INFO

Keywords:
Solid-state electrolyte
Li metal battery
Shape memory effect
High nickel cathode

ABSTRACT

Solid-state electrolytes (SSEs) are essential materials in all-solid-state lithium-metal batteries. However, a comprehensive SSE possessing high ionic conductivity, broad electrochemical window, and high thermal stability remains elusive. In this work, a novel bi-phase SSE featuring a shape memory effect is developed by in-situ thermal cross-linking of 2-ethyl cyanoacrylate (CA), polyethylene glycol methyl ether acrylate (PEGMEA), succinonitrile (SN), and fluoroethylene carbonate (FEC) additives. Due to the phase separation phenomenon and interfacial Li-ion conduction, the bi-phase SSE exhibits a room-temperature ionic conductivity of 1.9 mS cm^{-1}. Meanwhile, the bi-phase SSE exhibits a high oxidation potential of 4.9 V (vs Li/Li^+), and a lithium-ion transference number (t_{Li+}) of 0.56. Coupling with $LiNi_{0.8}Co_{0.1}Mn_{0.1}O_2$ (NCM 811) cathode and 11 μm bi-phase SSE, solid-state lithium metal batteries (SSLMBs) demonstrate long-term cycling stability (capacity retention > 92% after 250 cycles), excellent rate performance (126 mA h g^{-1} at 2 C, and high-voltage stability (208 mA h g^{-1} at 4.5 V). This investigation demonstrates the potential of bi-phase SSEs as a promising material for the development of high-performance SSLMBs.

1. Introduction

The demand for high-capacity, high-density, and miniaturized batteries is steadily rising in line with the imperative of achieving a carbon-neutral society [1]. Polymer-based solid-state Li metal batteries high energy density and high safety have emerged as one of promising candidates for next-generation batteries [2,3]. As the crucial material, a variety of solid polymer electrolytes (SPEs) have been developed in recent years, such as, polyether (PEO) [4], polyester [5], and polycarbonates [6]. Among the common SPEs, polyethylene oxide (PEO) based polymer electrolytes have shown promise due to their flexibility and good lithium anode stability. Unfortunately, the oxidation stability of PEO-based SPEs is constrained by the onset of the oxidation of the ethylene oxide (EO) segment above 3.9 V voltage [7]. Introducing functional-group into polymer chains (such as fluorinated-PEO) may be a feasible method to obtain high voltage stability and increased safety for PEO-based polymer electrolytes [8]. However, this simple introduction of the functional-group polymer chain does not lead to a significant improvement in the oxidation stability (less than 4.5 V), and the ionic conductivity of modified PEO is still far from application [9–11].

To address the oxidation stability of SPE, a novel elastomer electrolyte was developed by in-situ polymerization of cyano-group containing 2-cyanoethyl acrylate (CA) with EO segment monomer poly (ethylene glycol) methyl ether acrylate (PEGMEA) [12]. Also, CA shows an excellent mechanical support and a good high affinity to Li metal because CA usually serves as a main component for super glue with high adhesive properties [13]. The cross-linked polymer forms a three-dimensional polymer network, offering high oxidation stability against $LiCoO_2$ (4.4 V), high mechanical strength and good interface stability against Li metal [9]. Unfortunately, the ionic conductivity of such elastomer based polymer electrolyte exhibit a relative low level (0.01 mS cm^{-1} at room temperature) due to the high viscosity. To further improve the ionic conductivity of SPEs, Succinonitrile (SN) is normally employed an effective plasticizer due to its high acceptor number, a low molecular weight, and high oxidation potential [14–17].

* Corresponding authors.
E-mail addresses: xiehm136@nenu.edu.cn (H. Xie), xsun9@uwo.ca (X. Sun), liuyl290@nenu.edu.cn (Y. Liu).

https://doi.org/10.1016/j.nanoen.2023.109054
Received 9 August 2023; Received in revised form 7 October 2023; Accepted 30 October 2023
Available online 2 November 2023

Resultantly, SN-based plastic crystal electrolyte (PCE) gives a high lithium-ion conductivity (>5 mS cm^{-1}). Unfortunately, the previously reported PEO-PCE composite still falls short of the required standards in terms of ionic conductivity and mechanical strength [18,19]. Therefore, the state-of-the-art SPEs suffer from either a narrow electrochemical window or inferior electrochemical properties at ambient temperature, thus limiting their suitability to match both lithium metal anodes and high voltage cathodes [4]. Therefore, it is urgent to find a novel polymer-based SPE with both higher voltage compatibility (>4.5 V), higher ionic conductivity (>1 mS cm^{-1}) and good mechanical properties (>200 MPa).

In this work, we report a polymer bi-phase SSEs, which is prepared by in-situ thermal induced cross-linking polymerization of elastomer monomer CA, EO monomer PEGMEA and high conductive SN phase. By employing a two-step mixing approach, PCE is uniformly dispersed within the polymer matrix, resulting in the establishment of continuous three-dimensional pathways for efficient lithium transport. As a result, the electrolyte exhibits a high room temperature ionic conductivity (1.9 mS cm^{-1}) at good elastomer/PCE volume ratio (1:1), which is higher than Janus SPE electrolytes (0.35 mS cm^{-1}) [20]. Furthermore, the electrolyte demonstrates remarkable resistance to oxidation (4.9 V, as ascertained through voltage floating tests and linear scanning voltammetry) when maintaining an 11 μm thickness. Moreover, the designed bi-phase electrolyte possesses a shape memory feature, allowing it to restore its shape after triggering brief deformation through external stimulation such as temperature. The Li//Li symmetric battery with CA-PEGMEA-SN electrolyte runs stable for 1600 h at 0.1 mA cm^{-2}, with a critical current density of 0.5 mA cm^{-2}. High voltage $LiNi_{0.8}Co_{0.1}Mn_{0.1}O_2$(NCM 811)//Li full battery employed with CA-PEGMEA-SN achieves high interfacial stability at a high loading of

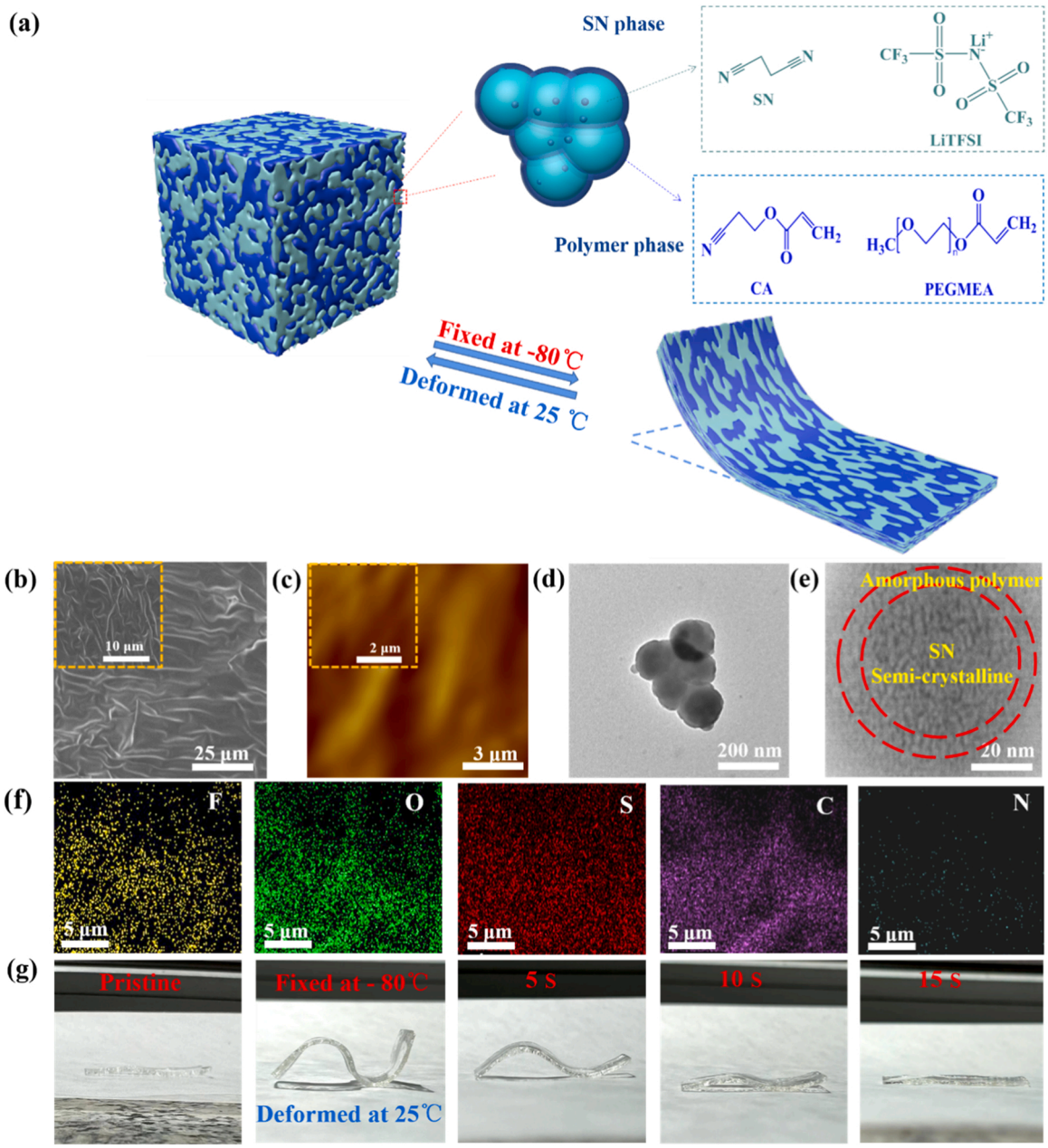

Fig. 1. (a) Illustration of the micro-structure of the CA-PEGMEA-SN solid polymer electrolyte (b) SEM images of CA-PEGMEA-SN(c) AFM images CA-PEGMEA-SN (d-e) TEM images of CA-PEGMEA-SN(f) corresponding EDS mappings of the SEM image in Fig. 1b (g) Solid electrolytes are edited into S forms to demonstrate shape memory function.

12 mg cm^{-2} and cutting-off voltage of 4.5 V. Also, the SPE based Li metal battery shows good rate capability and cycling reversibility in a wide temperature range of − 2–50 ^{0}C. This work underscores the potential of the biphasic SSEs as an enabling material for high-performance solid--state batteries, offering enhanced safety, stability, and versatility.

2. Results and discussion

The photographs of precursor solutions with different proportions of plastic electrolyte and elastic polymer are depicted in Fig. S1. All precursors are in the state of transparent dilute solution at ambient temperature. The physical form of the solution changes enormously after thermal polymerization at 80 °C. As shown in Fig. 1a, the precursor solution becomes solid with PEGMEA(CA): SN(FEC)= 1:1 by cross-linking reaction of CA and PEGMEA. However, the precursor solution with a volume ratio of 2:1 and 3:1 remains in a liquid state after the thermal polymerization process because of a higher SN content (Fig. S1).

The ionic conductivity of the solid polymer electrolytes (SPEs) is one of the crucial factors affecting SPES's electrochemical properties. Solid Electrolyte (PEGMEA (CA): SN (FEC) = 1:1) shows a room temperature ionic conductivity of 1.9 mS cm^{-1} (Fig. S2). With the assistance of a polyethylene (PE) separator, the mechanical strength of SPE is increased significantly (as discussed in Fig. 2). However, it leads to a decrease in conductivity due to the blocking effect of the PE structure. Fig. S3 shows the room temperature ionic conductivity with different ratios of PEGMEA(CA): SN(FEC) with PE as support. The ionic conductivity of electrolytes increases with the increased content of SN. Herein, SN not only reduces the crystallinity of the elastic polymer but also directly participates in the transport process of Li ions [21]. Considering the balance of mechanical and ionic conductivity, the ratio of precursor solution is fixed at 1:1(PEGMEA(CA):SN(FEC)) in the subsequent study.

Polyethylene-supported solid-state electrolyte membranes are prepared through an in-situ polymerization process with a thickness of 11 μm (Fig. S1 and Scheme S1). The original porous PE separator is successfully filled with a large amount of solid polymer electrolyte (Fig. S4). Morphologies of solid electrolytes are investigated by scanning electron microscopy (SEM). The synthesized SPE exhibits a three-dimensional structure of a bricks-like polymer phase, as shown in Fig. 1b. The atomic force microscopy (AFM) images of SPE also shows that the cross-linked polymer forms a wrinkled texture in the whole framework with a domain size of 1 μm width (Fig. 1c). Detailed information of the polymer structure is revealed with transmission electron microscopy (TEM) in Fig. 1d. Solid electrolytes consist of spherical particles with a diameter of 100 nm. Furthermore, high-resolution images in Fig. 1e confirm that the nano-structure of solid electrolyte is composed of a semi-crystalline SN phase and an amorphous polymer phase. Such a nano-phase separation phenomenon greatly constrains the growth of a high conductive SN phase (core phase) through the polymer (shell phase). Thus, numerous interfaces are formed between the conductive and elastic polymer phase (CA-PEGMEA) and the highly conductive SN phase, which facilitate fast ion transportation. As a result, the ionic conductivity can be largely increased. The bi-phase electrolyte exhibits much higher ionic conductivity than the pure elastic PEO electrolyte (Table S1). The uniformity of the solid electrolyte membrane is further confirmed by the energy dispersive spectroscopy (EDS) mapping images of the CA-PEGMEA-SN, as shown in Fig. 1f.

Shape memory materials are a highly desirable category of materials with remarkable properties, enabling them to respond to external

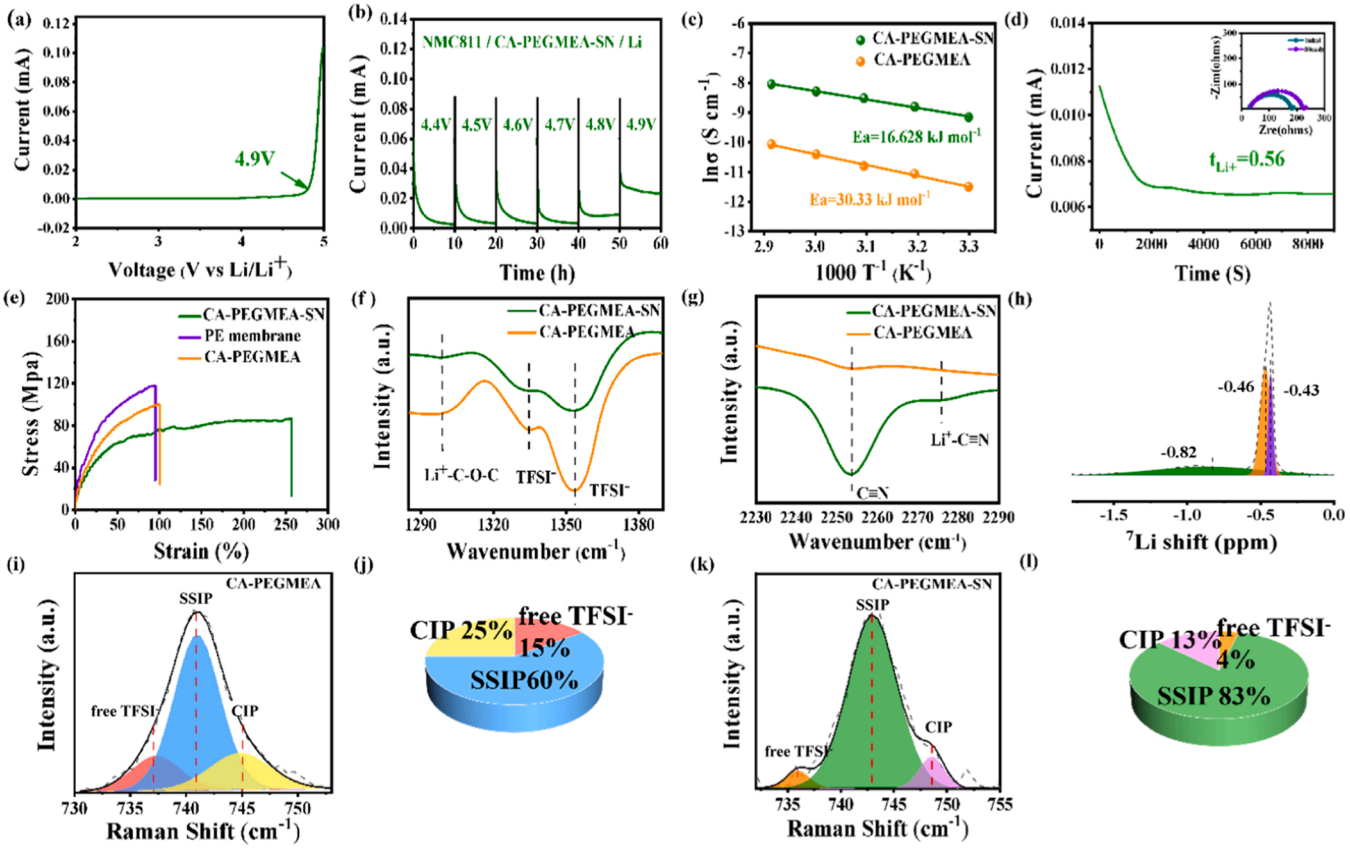

Fig. 2. (a) LSV curves of the CA-PEGMEA-SN with a scan rate of 0.1 mV s^{-1}. (b) The cell was charged to 4.4 V at 0.05 C (Loading=5 mg) and then held at gradually higher voltages for 10 h up to 5.0 V. (c) Linear fit of ln (σ_i) using the Arrhenius model. (d) Li/CA-PEGMEA-SN/Li symmetrical cell for transference number test. (e) Tensile stress-strain curves of PE membrane, CA-PEGMEA and CA-PEGMEA-SN. (f) FTIR spectra of CA-PEGMEA-SN and CA-PEGMEA in the 1280–1380 cm^{-1} range. (g) FTIR spectra of the polar C≡N stretching vibrations in the CA-PEGMEA-SN and CA-PEGMEA (h) ^{7}Li solid-state NMR spectra of CA-PEGMEA-SN (i-j) Raman spectra obtained from CA-PEGMEA in the range of 730–760 cm^{-1} range. (k-l) Raman spectra obtained from CA-PEGMEA in the 730–760 cm^{-1} range.

stimuli and exhibit programmable shape memory behaviors.[22,23] These materials can retain a permanent shape, deformed and fixed into a minor, temporary shape, and subsequently restored to their original, permanent shape through the application of external stimuli such as temperature, light, and magnetic field. The unique shape memory property of CA-PEGMEA-SN offers solutions to various existing challenges, such as repeated cycles adapted to mechanical deformation in practice. Differential Scanning Calorimeter (DSC) is used to measure the glass transition temperature (T_g), which is applied as the transition temperature for the shape memory effect. The glass transition temperature (as shown in Fig. S5) of CA-PEGMEA-SN is measured to be − 68 ℃. Thus, − 80 ℃ is chosen as the shape-fixing temperature to regulate the temporary shape of the CA-PEGMEA-SN. The membrane is first placed at approximately − 80 ℃ for 3 min to fix it into a temporary shape of 'S' type. Upon the solid electrolyte returning to room temperature, the 'S' shape is unfolded and restored to its original permanent shape (Fig. 1g). Further validation of the shape memory effect is demonstrated in Fig. S7, where the shape of an 'O' is temporarily formed and subsequently restores to its initial state within 25 s. The shape recovery behavior is attributed to the solid electrolyte with a soft segment (PEGMEA-CA) and the hard segment (SN) between − 80 ℃ and 25 ℃.

2.1. Characterization of bi-phasic electrolyte

The oxidative stabilities of the CA-PEGMEA electrolyte and CA-PEGMEA-SN electrolyte were evaluated by linear sweeping voltammetry (LSV) test using Li//SS cells. The CA-PEGMEA-SN electrolyte exhibits an oxidation potential of 4.9 V while the CA-PEGMEA is only 4.46 V, which is attributed to the introduction of high-voltage resistant plastic crystal electrolyte (PCE) (Figs. 2a and S8). To further verify the oxidation stability of the electrolyte, the leakage current at different cut-off voltages was performed. As shown in Fig. 2b, NCM 811// Li cell with CA-PEGMEA-SN is charged at a voltage range from 4.4 to 4.9 V in a 0.1 V stepwise ramp, and the voltage is kept at a targeted value for 10 h. The measured leakage current remains at less than 10 μA until 4.9 V (Fig. 2b), suggesting less interface side-reaction in cells [24]. The result is consistent with the linear-sweep voltammetry results, indicating an oxidation voltage of 4.9 V at the cathode interface(Fig. 2a).

Due to the formation of a bi-phasic structure, the room temperature ionic conductivity is increased to 0.19 mS cm^{-1}, which is 19 times higher than CA-PEGMEA electrolyte (0.0102 mS cm^{-1}) (Fig. S9 and Table S1). As shown in Fig. 2c, the ion conductivity changes against temperature are evaluated and recorded from 30° to 70°C, which can be fitted with the Arrhenius equation. The activation energy (E_a) of the CA-PEGMEA-SN electrolyte is estimated to be 16.628 kJ mol^{-1}, lower than that of the CA-PEGMEA electrolyte (30.33 kJ mol^{-1}). The results suggest that the ion conduction pathway of continuous PCE domain with high conductivity is formed.

Lithium transference number (t_{Li+}) is a critical parameter for solid electrolyte materials[25], especially in Li metal batteries. CA-PEGMEA-SN electrolyte exhibits a lithium-ion transference number (t_{Li+}=0.56) (Fig. 2d), which is five times higher than that of CA-PEGMEA electrolyte (t_{Li+} =0.117) (Fig. S10). The high t_{Li+} value is crucial to enable fast charging of LMBs. Tg is an important factor affecting ion migration, which is associated with the crystallinity of the solid electrolyte. Fig. S5 presents the DSC curve of CA-PEGMEA-SN and CA-PEGMEA from − 80–200 ℃. The Tg and Tm value of the polymer is shifted to a lower temperature with the addition of SN. This is due to the inhibition of the crystallization of PEGMEA after the addition of SN. The mechanical elasticity of CA-PEGMEA-SN and CA-PEGMEA electrolytes is demonstrated by tensile tests. CA-PEGMEA-SN electrolyte shows an excellent elongation ratio of approximately 258%, whereas CA-PEGMEA electrolyte only shows an elongation rate of around 100% (Fig. 2e). Thermal stability of the polymer electrolyte was analyzed the by TG test in air, as shown in Fig S6, the solid electrolyte decomposition is divided into several parts. Firstly, FEC additive in PCE is burning out at 130 ℃, which is followed by the SN molecule. Later, CA-PEGMEA polymer start to decomposes as the temperature reaches 333.89 ℃. As temperature higher than 400 ℃, Li salt decompose into pieces. However, this electrolyte is still stable than the conventional electrolyte.

The ionic conduction mechanism of electrolytes is further investigated by FTIR. As shown in Fig. S11, the C═C peak disappears in the range of 1600–1660 cm^{-1}, demonstrating the full polymerization of CA and PEGEMA monomers in the raw materials. As shown in Fig. 2f, a Li-(C-O-C) peak emerges at 1300 cm^{-1}, which implies the existence of an interaction between the Li ions and the ether group (Li-PEGEMA). This Li-(C-O-C) peak is also observed at 1080 cm^{-1} and 1650 cm^{-1}, with or without SN addition (Fig. S12).[26] Interestingly, the two peaks at 2254 cm^{-1} and 2275 cm^{-1} correspond to the free SN and the Li-coordinated SN, respectively, indicating the involvement of SN in the conduction path [27,28]. Compared to CA-PEGEMA, the bi-phasic electrolyte design contains a double lithium conduction path. To better demonstrate the unique lithium-ion transport behavior of CA-PEGMEA-SN, a ^{7}Li solid-state nuclear magnetic resonance (NMR) spectroscopy analysis is performed (Fig. 3h), The ^{7}Li resonance of the CA-PEGMEA-SN is resolved into three peaks attributed to the lithium-ion conduction in CA-PEGMEA based elastomer (−0.43 ppm), SN PCE electrolyte (−0.82 ppm) and interaction between the elastomer/SN interface (−0.46 ppm). The SN molecules have a very high dielectric constant (ε is about 55) and can effectively dissociate the lithium salt [29]. The addition of succinonitrile effectively inhibits the crystallization of PEGMEA-CA and weakens the binding force between oxirane and lithium ions, forming a new ion channel and realizing the conduction path of lithium. The transport modes of lithium-ion in two types of electrolytes are further illustrated in Fig. S13, which highlights that the Li^+ conducting pathways in CA-PEGMEA-SN involve both the elastic polymer phase (CA-PEGMEA) and the high conductive plastic crystal phase SN.

To explore the electrolyte structure, Raman spectroscopy is employed to examine the CA-PEGMEA-SN and CA-PEGMEA, in the frequency range of 730–760 cm^{-1}. Based on the fitting results, the CA-PEGMEA-SN electrolyte exhibits a significant presence of solvent-separated ion pairs (SSIPs) structures, accounting for 83% of the solvation structure. This value is higher than that of CA-PEGMEA electrolyte (60%), resulting in a high conductive microstructure. In addition, the percentage of close ion pairs (CIP) structure in the CA-PEGMEA-SN electrolyte is observed to be lower (13%) compared to the CA-PEGMEA electrolyte (25%) (Fig. 2i-l Table 2). This indicates that a high percentage of lithium salt is dissociated in the bi-phase electrolyte. According to previous reports, free $TFSI^-$ accelerates the oxidation and decomposition of the electrolyte itself [30]. CA-PEGMEA electrolyte with high content of free TFSI anions is easily oxidized, inconsistent with LSV result.

2.2. Lithium deposition behavior

Motivated by the exceptional mechanical and electrochemical properties of the CA-PEGMEA-SN electrolyte, we performed Li plating and stripping tests in symmetric Li cells (Fig. 3a). As shown in Fig. 3a, the overpotential of lithium metal cells increases rapidly at 40 h in the Li /CA-PEGMEA/ Li cell. A significant and irreversible voltage drop occurs after 50 h, which may be attributed to a short circuit caused by dendrite growth. In contrast, the Li /CA-PEGMEA-SN/Li cell maintains a stable cycle for 400 h with a polarization voltage below 80 mV at a current density of 0.2 mA cm^{-2}. Meanwhile, a low overpotential plateau of only about 25 mV is observed at 0.1 mA cm^{-2} (Fig. 3b). Moreover, the overpotential is stable at different current densities, with over-potential values of 50, 100 and 160 mV at 0.2, 0.3 and 0.5 mA cm^{-2}, respectively.

To investigate the interface stability, the time evolution in interfacial resistance of the CA-PEGMEA-SN is examined by monitoring the impedance response at ambient temperature under OCV conditions. As shown in Fig. 3c, the real part of the highest frequency impedance

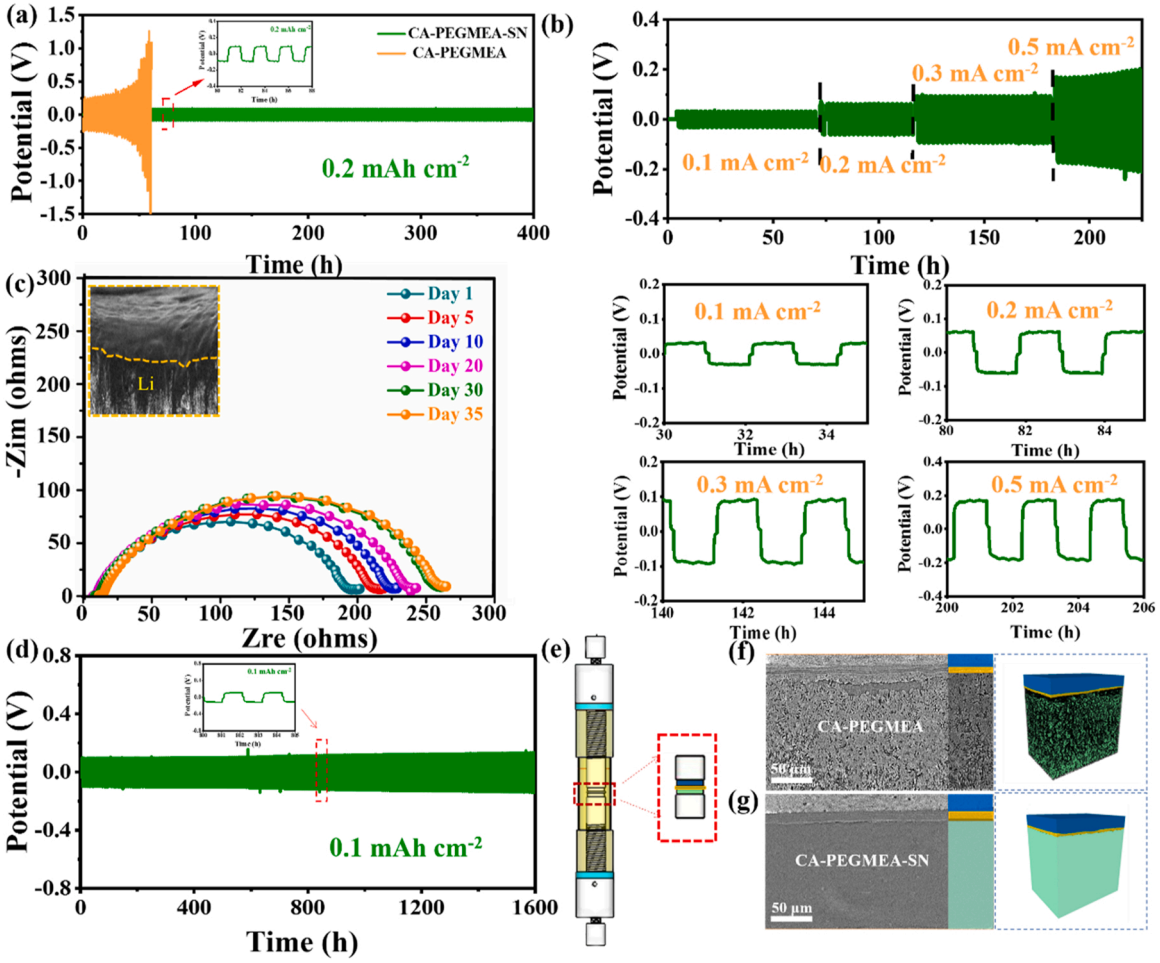

Fig. 3. (a) The voltage profiles of Li//Li symmetric batteries with CA-PEGMEA-SN and CA-PEGMEA at 0.2 mA cm^{-2} (b) The voltage profiles of Li//Li symmetric batteries with CA-PEGMEA-SN at different current density. (c) Nyquist plots of the interfacial resistance with time for CA-PEGMEA-SN using the Li/CA-PEGMEA-SN/Li symmetric cell (d). The long-term voltage profiles of Li//Li symmetric batteries with CA-PEGMEA-SN at 0.1 mA cm^{-2} (e)A schematic illustration of the synchrotron X-ray tomography technique and the battery components inside the tomography cell. (f) Reconstructed X-ray tomography slice and the 3D rendering of the Li|CA-PEGMEA|NMC622 cell after cycles. (g) Reconstructed X-ray tomography slice and the 3D rendering of the Li|CA-PEGMEA-SN|NMC622 cell after cycles.

represents the bulk resistance of the electrolyte (R_{SPE}), and the diameter of capacitive arcs is related to the interface resistance of the electrolyte with electrodes (R_{SEI}). Initially, the fresh battery shows an R_{SPE} of 7.52 Ω and an R_{SEI} of 201.7 Ω. Over time, the resistance of the R_{SEI} increases slowly due to the formation of the passivation layer. On the 30th day, R_{SEI} reaches 234.5 Ω and is unchanged at the 35th day. It indicates that the stable SEI layer is formed on the Li metal. The stable SEI layer provides excellent interfacial performance and guarantees closer contact between the electrolyte membrane and the lithium anode, which is the basis for the uniform deposition of lithium and suppression of lithium dendrite growth. SEM is used to observe the negative electrode cross-section of the battery, as shown in the inset of Fig. 3c. It reveals that CA-PEGMEA-SN is in seamless contact with the lithium sheet, and the solution undergoes in-situ thermal polymerization along the surface, forming a flat and stable interface. To evaluate the anode long-term cycling stability of CA-PEGMEA-SN electrolyte, Fig. 3d demonstrates that the Li /CA-PEGMEA-SN/ Li cell maintains a stable cycle for 1600 h at a current density of 0.1 mA cm^{-2} (with a polarization voltage of 100 mV using a thicker film of 40 μm). Our result is superior than the "Ceramic in Ionogel" SPE electrolytes in terms of cycling time (800 h) [31].

Furthermore, X-ray tomography of synchrotron radiation is used to study the lithium plating/striping behavior in Li | CA-PEGMEA| NMC622 and Li | CA-PEGMEA-SN | NMC622 cells (Fig. 3e). Fig. 3f shows the cross-section and the 3D rendering of the cell with CA-PEGMEA electrolyte. Due to its serious side reactions, the Li metal deposits show an enormous amount of porous and rough structure after cycling. These deposits are mostly electrochemically inert "dead Li" after repeated plating/stripping, causing continuous capacity decay. [32] In addition, the electrolyte (yellow circuit region) is also twisted due to the formation of the porous lithium, which induces a big volume change. In contrast, Li | CA-PPEGMEA-SN | NMC622 cells result in uniform lithium deposition, as seen in Fig. 3g. The Li metal still keeps an integrity and dense structure without breakage or void. The middle electrolyte layer keeps in a flat shape because there is no volume expansion. The stable Li deposition ensures the long-term cycle stability of CA-PEGMEA-SN electrolyte.

2.3. Battery performance under high-voltage conditions

The electrochemical performance of the CA-PEGMEA-SN and CA-PEGMEA electrolyte in the full cell is evaluated with NCM 811 (and NCM 622) cathode and Li metal anode through an in-situ build process. As shown in Fig. 4a, with an NCM 622 active mass loading of 3 mg cm^{-2}, the CA-PEGMEA-SN exhibits an initial discharge capacity of 166 mA h g^{-1} at 0.1 C for CA-PEGMEA-SN. After 250 cycles, the discharge capacity of CA-PEGMEA-SN remains at 152 mA h g^{-1}, corresponding to a capacity retention of 92%. In contrast, CA-PEGMEA has an

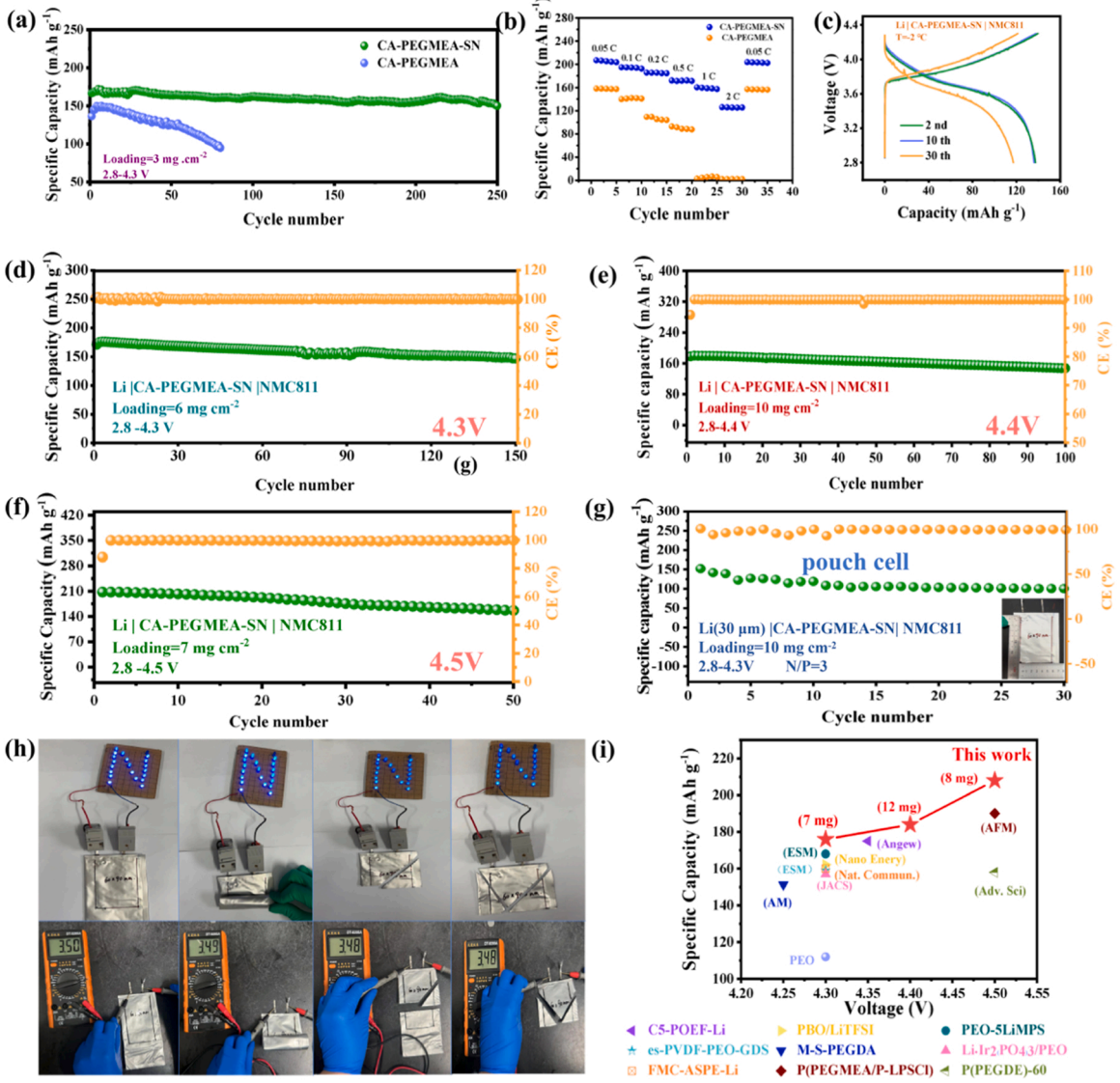

Fig. 4. (a) Cycling performance of the cell for CA-PEGMEA-SN and CA-PEGMEA with NCM 622. (b) Rate capability of NMC811/Li cell using different ratio of CA-PEGMEA-SN and CA-PEGMEA. (c) charge/discharge voltage profiles of Li/CA-PEGMEA-SN/NCM 811 battery at − 2 °C. (d) Cycling performance of the cell for CA-PEGMEA-SN with NCM 811 at 0.05 C and a cutoff voltage 4.3 V. (e) Cycling performance of the cell for CA-PEGMEA-SN with NCM 811 at a cutoff voltage 4.4 V. (f) Cycling performance of the cell for CA-PEGMEA-SN with NCM 811 at a cutoff voltage 4.5 V. (g) Cycling performance of the soft pack battery. (h) Battery safety test in pouch cell. (i) Performance comparison of previous report solid polymer electrolyte (C5-POE (C5-POEF), PBO, PEO-$Li_{0.46}Mn_{0.77}PS_3$(LiMPS), PVDF-PEO-GDC(CeO_2), branched solid polymer electrolyte (M-S-PEGDA), CPE-05MC (PEO-$Mg(ClO_4)_2$), P(PEGMEA/P)-LiPSCl(Li_6PS_5Cl), FMC-ASPE-Li, P(PEGDE)-$Li_{10}GeP_2S_{12}$) [34–43].

initial discharge capacity of 135 mA h g^{-1} and a specific discharge capacity of 81 mA h g^{-1} after 70 cycles. Clearly, CA-PEGMEA-SN exhibits excellent discharge capacity retention in the cycle, while CA-PEGMEA exhibits a severe decay in charge/discharge capacity. The difference can be attributed to the ionic conductivity and t_{Li+}. Fig. 4b shows the rate performances at various current densities, with a voltage range of 2.8–4.3 V. The specific discharge capacity is reduced with the increase of current density because of kinetic limitations. The CA-PEGMEA-SN electrolyte exhibits better performance at different current densities, especially at a high rate of 2 C, and delivers a discharge capacity of 126 mA h g^{-1}, which is significantly higher than that of the NCM 811 /CA-PEGMEA/ Li cells (0.5 mA h g^{-1}, 2 C). This is mainly due to the good ionic conductivity and interfacial compatibility of CA-PEGMEA-SN electrolytes.

An NCM 811 cathode sheet with higher mass loading was prepared with a cut-off voltage of 4.3–4.5 V. As shown in Fig. 4d, at an active mass loading of 6 mg cm^{-2} and within a voltage range of 2.8–4.3 V, the initial discharge capacity of the NCM 811 cathode shows 171 mA h g^{-1} at 0.05 C. After 150 cycles, the discharge capacity reach 146 mA h g^{-1}, corresponding to a capacity retention of 85.2%. Fig. 4e shows the NCM 811 cathode with an active mass loading of 10 mg cm^{-2} and a cut-off voltage of 4.4 V. The initial discharge capacity is increased to 178 mA h g^{-1} at a higher de-lithiation state. The discharge capacity drops to 147 mA h g^{-1} at the 100th cycle, with a capacity decay of 0.3 mA h g^{-1} per cycle. Such high voltage compatibility is better than biomimetic channels inspired electrolytes (4.4 V, 50th, 80%) [33]. At a cut-off voltage of 4.5 V (Fig. 4f), the initial discharge capacity reaches 208 mA h g^{-1}, which is very close to the liquid cell with a high de-lithiation state. After 50 cycles, the discharge capacity decreases to 157 mA h g^{-1} and the Coulombic efficiency is about 100%. The results demonstrate that our bi-phase structure solid polymer electrolyte is high-voltage compatible. Additionally, the solid-state NCM 811 /CA-PEGMEA-SN/ Li pouch cell (0.11 Ah) with an ultra-thin Li anode of 30 μm is manufactured and tested to demonstrate the applications of the batteries. As shown in Fig. 4g, under an active mass loading of 10 mg cm^{-2} (N/P = 3), the NMC 811 pouch cell exhibits an initial

discharge capacity of 152 mA h g^{-1} at 0.1 C rate. After 30 cycles, the discharge capacity decreases to 100 mA h g^{-1} and the Coulombic efficiency is around 99%. The electrochemical performance was evaluated not only at room temperature but also at high temperatures (50 ℃) and low temperatures (−2 ℃). Fig. S13 shows the NMC 811 /CA-PEGMEA-SN/ Li cells with a voltage range of 2.8–4.3 V, the initial discharge capacity is 188 mA h g^{-1} at 50 ℃. A discharge capacity of 122 mA h g^{-1} is achieved after 150 cycles at 50 ℃, with a capacity retention of 65%. Figs. 4c and S15 show NMC 811 /CA-PEGMEA-SN/ Li cells performance at − 2 ℃, the initial discharge capacity is 139 mA h g^{-1}. After 12 cycles, the discharge capacity of 136 mA h g^{-1} and Coulombic efficiency of 100% are achieved. The discharge capacity reaches 119 mA h g^{-1} after 30 cycles, corresponding to a capacity retention of 86%. This proves that solid electrolytes also have excellent electrochemical properties over a wide temperature range.

Battery safety is also crucial for solid-state lithium metal batteries. To investigate the safety performance of pouch cells under mechanical abuse conditions, a bending test and corner-cut test were conducted on the NMC 811 /CA-PEGMEA-SN/ Li pouch cell. As shown in Fig. 4i, the pouch cell is capable of lighting up a commercial blue LED lamp under ambient conditions. After bending at 180° and cutting into pieces, the cell exhibits a minimal voltage decline and still successfully lights the lamp. Additionally, a corner piece cut from the NMC 811/PEGMEA-SN/ Li pouch cell is still able to light up the blue LED lamp, indicating no internal short circuit and showing good safety characteristics.

2.4. Interface analysis

To disclose the underlying reasons for the enhanced cycling stability of CA-PEGMEA-SN over CA-PEGMEA, the as-employed polymer matrixes after the corresponding NMC 811 cathodes and Li after cycling were characterized and analyzed. The morphology of the cells is examined after 70 cycles to analyze interface composition. In Fig. 5a, the Li anode surface in the NMC 811 /CA-PEGMEA/ Li battery exhibits a rough surface with massive inactive lithium. In contrast, the surface of the lithium metal in the NMC 811 /CA-PEGMEA-SN/ Li batteries is

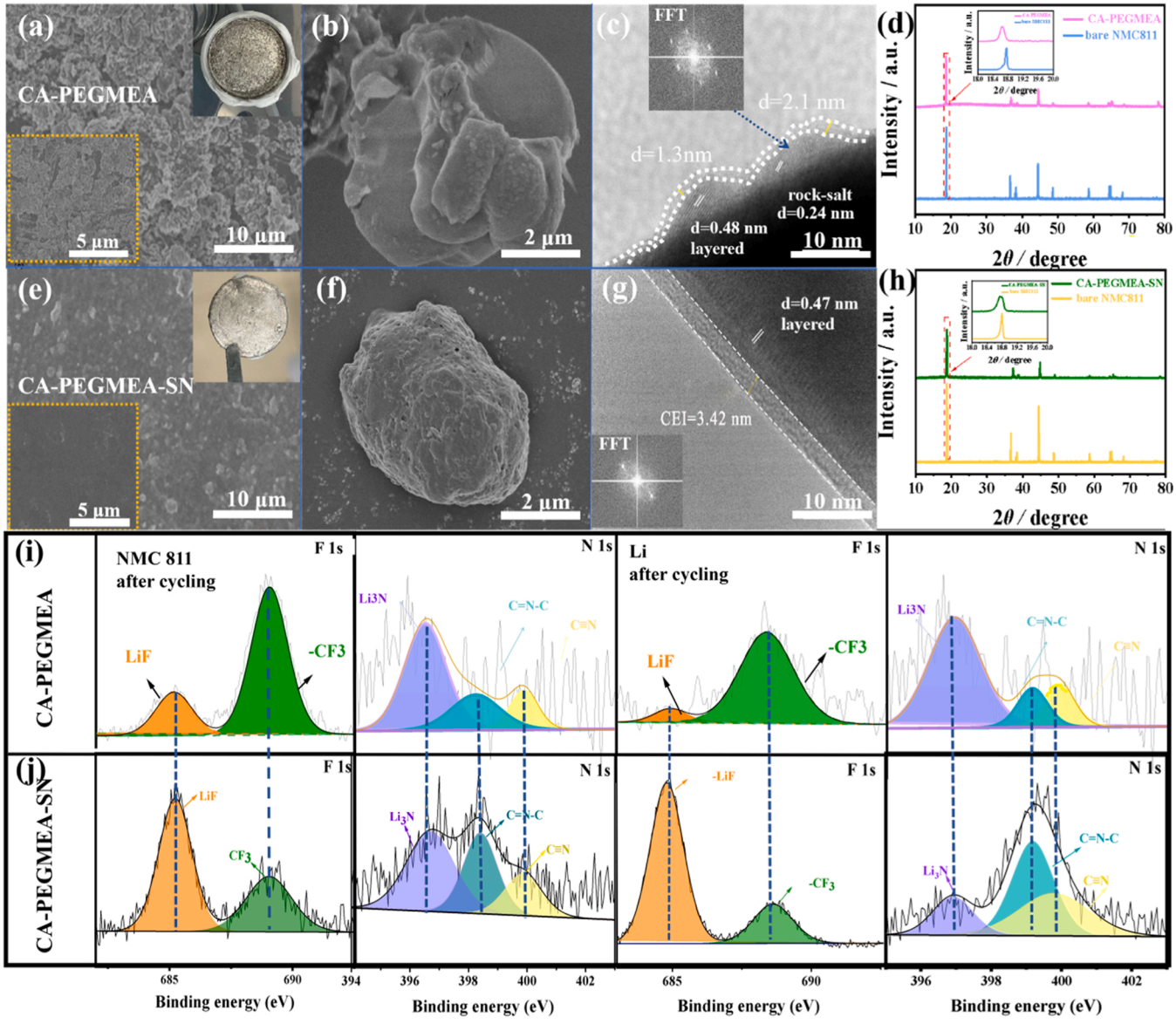

Fig. 5. (a, e) Plane SEM images of Li-metal obtained from NMC 811 /CA-PEGMEA/ Li and NMC 811 /CA-PEGMEA-SN/ Li cells after 70 cycles. (b, f) Typical SEM images of NMC811 particles after 70 cycles in NMC 811 /CA-PEGMEA / Li and NMC 811 /CA-PEGMEA-SN/ Li cells. (c, g) Typical TEM image of CEI layers of random areas on the surface of NMC 811 particles with CA-PEGMEA and CA-PEGMEA-SN after 70 cycles. (d, h) XRD results of NMC 811 with CA-PEGMEA and CA-PEGMEA-SN after 70 cycles. (i) XPS spectra of CA-PEGMEA after 70 cycles. (j) XPS profiles of CA-PEGMEA-SN after 70 cycles.

remarkably smooth, and no obvious dendrites or defects are observed. These results indicate that the Li metal anode cycled in CA-PEGMEA-SN maintains a relatively flat, dense and uniform morphology. Such structure and morphology of the Li metal anode confirm that CA-PEGMEA-SN exhibits excellent stability with Li metal anode, and the Li dendrite growth is effectively suppressed during charge/discharge cycles. This ensures good electrochemical performances of the high-voltage NMC 811 /CA-PEGMEA-SN/ Li batteries.

At the same time, the morphology of NMC 811 particles after cycling is characterized by SEM, as shown in Fig. 5b and f. Intergranular cracking of NMC 811 particles is observed after cycling in CA-PEGMEA electrolyte (Fig. 5f). It has been reported that such intergranular cracking of cathode particles can lead to serious capacity fade [44]. In contrast, the NMC 811 particles in CA-PEGMEA-SN retain integrity after the same cycling process (Fig. 5f). Additionally, XRD is also carried out to observe the change of the NMC 811 after cycling. It has been reported that the evolution of the (003) peak could reflect the change of NMC 811 crystal volume [45]. As shown in Fig. 5d, the (003) peak of NMC811 cycled in CA-PEGMEA moved towards the lower degree, which indicated a volume expansion due to irreversible structure change transition. On the contrary, the (003) peak of NMC 811 cycled in CA-PEGMEA-SN exhibits almost no change (Fig. 5h), which demonstrate better structural reversibility and integrity. To obtain more detailed information, NCM 811 particles are examined by TEM. NCM 811 particle in CA-PEGMEA shows both rock salt and layered phases, due to a surface structural change of NMC 811 crystals (Fig. 5c). In the NCM 811 lithiation state, divalent nickel ion (Ni^{2+}) tends to migrate from the transition metal layer to the lithium layer, resulting in a structure transition from the layer to the spinel phase and forming the rock salt phase [46]. In contrast, the NCM 811 particles in CA-PEGMEA-SN maintain their layered structure phase. Furthermore, the NMC 811 in CA-PEGMEA presents an irregular, loose CEI layer, whereas a dense and uniform CEI layer is observed on the NMC 811 in the CA-PEGMEA-SN with a thickness of only 3.42 nm (Fig. 5g). Moreover, this compact and uniform thin CEI can provide an effective Li^+ diffusion path, resulting in a higher cycling stability of NMC811 /CA-PEGMEA-SN/ Li cells than that of NMC811 / CA-PEGMEA / Li cells.

XPS is conducted to identify the chemical composition of CEI and SEI for CA-PEGMEA and CA-PEGMEA-SN electrolytes after cycling. CEI composition on NCM 811 cathode is obtained for two electrolytes, as shown in left two panels of Fig. 5i and j. A higher content of C═N-C film is detected for CA-PEGMEA-SN, in line with HRTEM images. Also, LiF (684.6 eV) signal observed on the cathode of CA-PEGMEA is lower, which means the oxidation reaction of polymer electrolyte is unsolved. As shown in right two panels of Fig. 5i and j, in terms of SEI on Li metal anode, large amount of electrolyte derived phase is formed during cycling. The N 1 s spectra can be deconvolved into three peaks 396 eV, 398.1 eV and 399.2 eV, corresponding to Li_3N, C-C═N and C≡N compounds, respectively. The formation of Li_3N can be attributed to the lithiation of the nitrile group of SN and CA. The presence of C-C═N indicates the polymerization of nitrile compounds on the Li surface from C≡N containing CA and SN. The F 1 s spectra at 686.8 eV represents C-F, and LiF at 684.6 eV signal is observed due to the decomposition of lithium salt. In comparison to CA-PEGMEA electrolyte, SEI layer in the CA-PEGMEA-SN electrolyte contains higher content of LiF and C-C═N than CA-PEGMEA, which build an organic-inorganic composite SEI layer. Also, a high content of lithium oxide is detected at O 1 s spectra in CA-PEGMEA-SN (Fig. S16), which is decomposition product of the bi-phase electrolyte. Such inorganic-rich SEI layer promotes rapid Li^+ migration at the interface, also facilitates the uniform deposition of Li^+ at the interface, thus stabilizing the Li anode/electrolyte interface.

To get insight into the CEI and SEI structure, XPS depth profiling was conducted for Li|CA-PEGMEA-SN|NMC811 cells after 20 cycles (Fig. S17). With the increase of etching time on the surface of Li, the content of inorganic phase such as LiF and Li_3N decreases, while the content of C-C═N increases. This indicates that SEI on Li metal show a gradient distribution along the depth. It is beneficial for the rapid Li^+ conduction with surface inorganic layer, and the bottom organic layer can protect Li metal from further side-reactions. For the CEI film on NMC811, there was no significant change in terms of LiF (683 eV), Li_3N (396.3 eV), and C-C═N content with increasing etching time, suggesting a uniform distribution. Such CEI film suggest that the oxidation of electrolyte is well-controlled at the cathode interface.

3. Conclusion

To summarize, a biphasic solid electrolyte demonstrating remarkable room temperature ionic conductivity (1.9 mS cm^{-1}) and a distinct shape memory trait has been successfully developed. This enhanced conductivity is attributed to nanoscale phase separation and interfacial lithium ion conduction. The robust adhesive properties of CA-PEGMEA-SN result in a closely bound lithium anode/electrolyte interface, fostering stable Li deposition over an impressive duration of 1600 h at 0.1 mA cm^{-2}. When combined with the NMC 811 cathode, this 11 μm bi-phase electrolyte achieves a noteworthy discharge capacity of 208 mA h g^{-1} at a 4.5 V cut-off voltage. Moreover, the NMC 811 // Li cell demonstrates exceptional stability across a wide temperature range, facilitating by the formation of a thin and dense CEI film on the cathode surface. This progress is further substantiated by the pouch cell's achievement of a remarkable energy density of 400 Wh/kg, employing a 30 μm Li metal and a high-loading (10 mg cm^{-2}) NCM 811 cathode configuration.

CRediT authorship contribution statement

Yulong Liu: Conceptualization, Project administration. **Yiqi Gong**: Methodology. **Yiqi Gong, Mingyang Xin, Pingbo Xu, Yulong Liu**: Validation. **Silin Chen**: Formal analysis. **Silin Chen, Pingbo Xu, Jia Liu, Dan Li**: Investigation. **Silin Chen, Pingbo Xu, Yulong Liu**: Data curation. **Yulong Liu, Haiming Xie, Yintong Wang, Changhong Wang**: Writing – original draft preparation. **Changhong Wang, Xueliang Sun**: Writing – review & editing. **Yulong Liu, Haiming Xie**: Supervision, Funding acquisition. All authors have read and agreed to the published version of the manuscript.

Declaration of Competing Interest

We declare that we have no financial and personal relationships with other people organizations that can inappropriate influence our work, there is no professional or other personal interest of any nature or kind in any product, service and/or company that could deconstructed as influence the position presented in, or the review of, the manuscript entitle.

Data availability

Data will be made available on request.

Acknowledgments

This work was supported by Jilin Province Science and Technology Department major science and technology project (No. 20220301004GX; No. 20220301005GX); Key Subject Construction of Physical Chemistry of Northeast Normal University (2412022XK004); National Natural Science Foundation of China (22102020). We thank Shanghai Synchrotron Radiation Facility (SSRF) for supporting the synchrotron X-Ray tomography measurement on Beamline BL13HB (the previous BL13W1 beamline) under the project (2020-SSRF-PT-012475).

Appendix A. Supporting information

Supplementary data associated with this article can be found in the

online version at doi:10.1016/j.nanoen.2023.109054.

References

[1] M. Li, J. Lu, Z. Chen, K. Amine, Adv. Mater. 30 (2018), 1800561.
[2] T.-Z. Hou, W.-T. Xu, X. Chen, H.-J. Peng, J.-Q. Huang, Q. Zhang, Angew. Chem. Int. Ed. 56 (2017) 8178–8182.
[3] X.-B. Cheng, R. Zhang, C.-Z. Zhao, Q. Zhang, Chem. Rev. 117 (2017) 10403–10473.
[4] H. Zhang, M. Armand, Isr. J. Chem. 60 (2020) 1–8.
[5] X. Pan, H. Sun, Z. Wang, H. Huang, Q. Chang, J. Li, J. Gao, S. Wang, H. Xu, Y. Li, W. Zhou, Adv. Energy Mater. 10 (2020), 2002416.
[6] J. Zhang, J. Zhao, L. Yue, Q. Wang, J. Chai, Z. Liu, X. Zhou, H. Li, Y. Guo, G. Cui, L. Chen, Adv. Energy Mater. 5 (2015), 1501082.
[7] C.F.N. Marchiori, R.P. Carvalho, M. Ebadi, D. Brandell, C.M. Araujo, Chem. Mater. 32 (2020) 7237–7246.
[8] Q. Wang, X. Liu, Z. Cui, X. Shangguan, H. Zhang, J. Zhang, K. Tang, L. Li, X. Zhou, G. Cui, Electrochim. Acta 337 (2020), 135843.
[9] Z. Lv, Q. Zhou, S. Zhang, S. Dong, Q. Wang, L. Huang, K. Chen, G. Cui, Energy Storage Mater. 37 (2021) 215–223.
[10] J. Chai, J. Zhang, P. Hu, J. Ma, H. Du, L. Yue, J. Zhao, H. Wen, Z. Liu, G. Cui, L. Chen, J. Mater. Chem. A 4 (2016) 5191–5197.
[11] M. Liu, H.R. Jiang, Y.X. Ren, D. Zhou, F.Y. Kang, T.S. Zhao, Electrochim. Acta 213 (2016) 871–878.
[12] Z. Liu, P. Hu, J. Ma, B. Qin, Z. Zhang, C. Mou, Y. Yao, G. Cui, Electrochim. Acta 236 (2017) 221–227.
[13] M.J. Lee, J. Han, K. Lee, Y.J. Lee, B.G. Kim, K.-N. Jung, B.J. Kim, S.W. Lee, Nature 601 (2022) 217–222.
[14] L.Z. Fan, Y.S. Hu, A.J. Bhattacharyya, J. Maier, Adv. Funct. Mater. 17 (2007) 2800–2807.
[15] K. Lee, H. Jung, J. Chung, K.S. Kim, J. Song, J. Park, Electrochim. Acta 281 (2018) 274–281.
[16] M.B. Effat, Z. Lu, A. Belotti, J. Yu, Y.-Q. Lyu, F. Ciucci, J. Power, Sources 436 (2019), 226802.
[17] K. Liu, Q. Zhang, B.P. Thapaliya, X.-G. Sun, F. Ding, X. Liu, J. Zhang, S. Dai, Solid State Ion. 345 (2020), 115159.
[18] W. Zha, J. Li, W. Li, C. Sun, Z. Wen, Chem. Eng. J. 406 (2021), 126754.
[19] Y. Liu, Y. Zhao, W. Lu, L. Sun, L. Lin, M. Zheng, X. Sun, H. Xie, Nano Energy 88 (2021), 106205.
[20] Q. Ruan, M. Yao, J. Lu, Y. Wang, J. Kong, H. Zhang, S. Zhang, Energy Storage Mater. 54 (2023) 294–303.
[21] J. Han, M.J. Lee, K. Lee, Y.J. Lee, S.H. Kwon, J.H. Min, E. Lee, W. Lee, S.W. Lee, B. J. Kim, Adv. Mater. 35 (2023), 2205194.
[22] V. Jabbari, V. Yurkiv, M.G. Rasul, M. Cheng, P. Griffin, F. Mashayek, R. Shahbazian-Yassar, Small 18 (2021), 2102666.
[23] Y. Huang, Z. Shi, H. Wang, J. Wang, Z. Xue, Energy Storage Mater. 51 (2022) 1–10.
[24] N.R. Vadivel, S. Ha, M. He, D. Dees, S. Trask, B. Polzin, K.G. Gallagher, J. Electrochem. Soc. 164 (2017) A508.
[25] P.R. Chinnam, S.L.J.J.o.M.C.A. Wunder, 1, 2013: pp. 1731–1739.
[26] H. Wu, Y. Xu, X. Ren, B. Liu, M.H. Engelhard, M.S. Ding, P.Z. El-Khoury, L. Zhang, Q. Li, K. Xu, C. Wang, J.G. Zhang, W. Xu, Adv. Energy Mater. 9 (2019), 1902108.
[27] L. Caradant, D. Lepage, P. Nicolle, A. Prébé, D. Aymé-Perrot, M. Dollé, ACS Appl. Polym. Mater. 2 (2020) 4943–4951.
[28] Z. Liao, J. Huang, W. Chen, N. Saito, Z. Zhang, L. Yang, S.-i Hirano, Energy Storage Mater. 33 (2020) 442–451.
[29] Q. Zhang, K. Liu, F. Ding, W. Li, X. Liu, J. Zhang, ACS Appl. Mater. Interfaces 9 (2017) 29820–29828.
[30] X. Chen, X.-Q. Zhang, H.-R. Li, Q. Zhang, Batter. Supercaps 2 (2019) 128–131.
[31] Q. Ruan, M. Yao, S. Luo, W. Zhang, C.-J. Bae, Z. Wei, H. Zhang, Nano Energy 113 (2023), 108571.
[32] F. Sun, M. Osenberg, K. Dong, D. Zhou, A. Hilger, C.J. Jafta, S. Risse, Y. Lu, H. Markötter, I. Manke, ACS Energy Lett. 3 (2018) 356–365.
[33] M. Yao, Q. Ruan, S. Pan, H. Zhang, S. Zhang, Adv. Energy Mater. 13 (2023) (pp).
[34] J. Luo, Q. Sun, J. Liang, X. Yang, J. Liang, X. Lin, F. Zhao, Y. Liu, H. Huang, L. Zhang, S. Zhao, S. Lu, R. Li, X. Sun, Nano Energy 90 (2021), 106566.
[35] H. Sun, X. Xie, Q. Huang, Z. Wang, K. Chen, X. Li, J. Gao, Y. Li, H. Li, J. Qiu, W. Zhou, Angew. Chem. Int. Ed. 60 (2021) 18335–18343.
[36] Y. Zhang, X. Sun, D. Cao, G. Gao, Z. Yang, H. Zhu, Y. Wang, Energy Storage Mater. 41 (2021) 505–514.
[37] B. Jiang, F. Li, T. Hou, Y. Liu, H. Cheng, H. Wang, D. Li, H. Xu, Y. Huang, Energy Storage Mater. 56 (2023) 183–191.
[38] L. Gao, S. Luo, J. Li, B. Cheng, W. Kang, N. Deng, Energy Storage Mater. 43 (2021) 266–274.
[39] H. Wang, Q. Wang, X. Cao, Y. He, K. Wu, J. Yang, H. Zhou, W. Liu, X. Sun, Adv. Mater. 32 (2020), 2001259.
[40] Y. Wang, J. Ju, S. Dong, Y. Yan, F. Jiang, L. Cui, Q. Wang, X. Han, G. Cui, Adv. Funct. Mater. 31 (2021), 2101523.
[41] Y. Su, X. Rong, A. Gao, Y. Liu, J. Li, M. Mao, X. Qi, G. Chai, Q. Zhang, L. Suo, L. Gu, H. Li, X. Huang, L. Chen, B. Liu, Y.-S. Hu, Nat. Commun. 13 (2022) 4181.
[42] F. Jiang, Y. Wang, J. Ju, Q. Zhou, L. Cui, J. Wang, G. Zhu, H. Miao, X. Zhou, G. Cui, Adv. Sci. 9 (2022), 2202474.
[43] B. Xu, X. Li, C. Yang, Y. Li, N.S. Grundish, P.-H. Chien, K. Dong, I. Manke, R. Fang, N. Wu, H. Xu, A. Dolocan, J.B. Goodenough, J. Am. Chem. Soc. 143 (2021) 6542–6550.
[44] H. Liu, M. Bugnet, M.Z. Tessaro, K.J. Harris, M.J.R. Dunham, M. Jiang, G. R. Goward, G.A. Botton, Phys. Chem. Chem. Phys. 18 (2016) 29064–29075.
[45] V. Riesgo-González, D.S. Hall, K. Märker, J. Slaughter, D.S. Wright, C.P. Grey, Chem. Mater. 34 (2022) 9722–9735.
[46] J. Zheng, Y. Ye, T. Liu, Y. Xiao, C. Wang, F. Wang, F. Pan, Acc. Chem. Res. 52 (2019) 2201–2209.

Yiqi Gong is a postgraduate Student of Department of Chem-Local United Engineering Laboratory for Power Battery. Her main research direction is the application of high-voltage resistant solid-state polymer electrolytes in lithium metal batteries.

Dr. Changhong Wang is now a tenure-track Assistant Professor at Eastern Institute of Technology (EITech), Ningbo. He received his MS degree in Material Engineering from the University of Science and Technology of China in 2014 and his PhD degree in Mechanical and Material Engineering from the University of Western Ontario in 2020. His current research interests include all-solid-state batteries, solid electrolytes, lithium-sulfur batteries, and solid-state pouch cells.

Mingyang Xin is a doctoral student at the National & Local United Engineering Laboratory for Power Battery, Northeast Normal University, China. His main research interests include the development of non-flammable liquid electrolytes, low-temperature electrolyte engineering and PVDF-based solid-state electrolytes for lithium-ion batteries.

Silin Chen is a Ph.D. student of Department of Chemistry at the Northeast Normal University and National & Local United Engineering Laboratory for Power Battery. Her main research interests include solid-state polymer electrolytes and high-voltage solid-state electrolytes.

Pingbo Xu is currently a Master of Engineering at Northeast Normal University and obtained his Bachelor's degree from Changchun University of Science and Technology in 2018. He specializes in the field of solid-state electrolytes for lithium-ion batteries, including polymer-based solid-state electrolytes and organic-inorganic composite solid-state electrolytes.

Dan Li is currently a Ph.D. student at Northeast Normal University. She received her Bachelor degree from Hebei Normal University in 2018. Her current research interests focus on electrode/electrolyte interfacial study of lithium-metal batteries.

Jia Liu is associate professor at Northeast Normal University, China. She received her Ph.D. degree on inorganic chemistry in Uppsala University of Sweden in 2015. Currently, she works on the development on functional materials on Li-S and Li-O_2 batteries.

Yintong Wang is currently studying at Xingjian Academy of Tsinghua University, China. He gained some experience by studying and working in State Key Laboratory of Tribology Tsinghua University. He participated in Prof. Yulong Liu's lab during the summer vocation on Li metal battery.

Haiming Xie is a professor of Department of Chemistry at the Northeast Normal University and the director of National & Local United Engineering Laboratory for Power Battery. He received his Ph.D. degree from Northeast Normal University in 2008. His main research interests include lithium iron phosphate cathode materials and heat-resistant separators for high safety and high-power lithium ion batteries, low-temperature power batteries and all-solid-state electrolytes for lithium batteries.

Prof. Xueliang (Andy) Sun is a Canada Research Chair in Development of Nanomaterials for Clean Energy, Fellow of the Royal Society of Canada and Canadian Academy of Engineering and Full Professor at the University of Western Ontario, Canada. Dr. Sun received his Ph.D. in materials chemistry in 1999 from the University of Manchester, UK, which he followed up by working as a postdoctoral fellow at the University of British Columbia, Canada and as a Research Associate at L′ Institut National de la Recherche Scientifique (INRS), Canada. His current research interests are focused on advanced materials for electrochemical energy storage and conversion.

Yulong Liu is currently associate professor at Northeast Normal University, China. Before working at Northeast Normal University, he was a postdoctoral fellow in Prof. Xueliang (Andy) Sun' Nanomaterials and Energy Group at the University of Western Ontario, Canada. He received his Bachelor degree from Central South University, China, in 2010, and Master degree in 2013. In 2018, he obtained his Ph.D. degree in Mechanical and Materials Engineering from University of Western Ontario. Previously, he worked together with GLABAT Solid State Battery Inc. on commercializing solid state batteries. His current research interests include nanomaterials for lithium ion batteries and high energy density solid-state lithium metal batteries.